





Electron Holography Details the Tagish Lake Parent Body and Implies Early Planetary Dynamics of the Solar System

Yuki Kimura¹ , Kazuo Yamamoto², and Shigeru Wakita^{3,4} ¹Institute of Low Temperature Science, Hokkaido University, Kita-19, Nishi-8, Kita-ku, Sapporo, 060-0819, Japan; ykimura@lowtem.hokudai.ac.jp²Nanostructures Research Laboratory, Japan Fine Ceramics Center, 2-4-1 Mutsuno, Atsuta-ku, Nagoya 456 8587, Japan³Department of Earth, Atmospheric, and Planetary Sciences, Purdue University, 550 Stadium Mall Drive, West Lafayette, IN 47907, USA⁴Department of Earth, Atmospheric and Planetary Sciences, Massachusetts Institute of Technology, 77 Massachusetts Avenue, Cambridge, MA 02139, USA

Received 2021 June 24; revised 2021 July 12; accepted 2021 July 12; published 2021 August 11

Abstract

The degree of aqueous alteration of small bodies in the solar system depends on the time of their formation, their size, and collisions with other bodies, among other factors. Therefore, a knowledge of the aqueous alterations recorded in meteorites is crucial to understanding the history of our solar system. The Tagish Lake meteorite, believed to have formed in the cold outer solar system, contains framboidal magnetite, a major product of the aqueous process. By in situ annealing experiments on the magnetic properties of the magnetite by electron holography and by numerical simulations, we show that the interior temperature of the parent body of the Tagish Lake meteorite reached $\sim 250^\circ\text{C}$ as a result of radiogenic heating and an energetic impact. Our nanometer-scale magnetic study suggested that the parent body grew to >160 km in diameter in the Kuiper Belt at ~ 3 Myr after the first solar system minerals formed and then experienced an energetic impact from a smaller body with a diameter of ~ 10 km at a speed of ~ 5 km s^{-1} about 4–5 Myr after the first minerals. The probability of such a high-impact-velocity event would have increased during travel of the parent body from the Kuiper Belt to the asteroid belt, triggered by the formation and migration of the giant planets. Our results imply the early dynamics of solar system bodies that occurred several million years after the formation of the solar system and a highly efficient formation of the outer bodies of the solar system, including Jupiter.

Unified Astronomy Thesaurus concepts: [Meteorites \(1038\)](#); [Planetary dynamics \(2173\)](#)

1. Introduction

In the early stages of the formation of the solar system, water played an important role in the mineralization (Grimm & McSween 1993; Rubin 2012) and in the modification of organics (Quirico et al. 2018) during the aqueous alteration of heated bodies of the solar system. Because the main heat source for these bodies is the heat of decay of short-lived radionuclides, older bodies of the solar system, which acquired larger amounts of heat sources (e.g., ^{26}Al ; $t_{1/2} = 0.74$ million years), could have reached higher interior temperatures than younger bodies. Therefore, to understand both the physical and chemical evolution of the solar system, it is crucial to study aqueous-alteration products in meteorites that are portions of small solar system bodies.

The Tagish Lake meteorite is a primitive chondrite with unique properties. Some samples of this meteorite experienced negligible alteration and minimal contamination on Earth as a result of their rapid recovery within a few days after falling in 2000 (Brown et al. 2000). Even the matrix of the pristine portions of the Tagish Lake meteorite contains magnetite, a major aqueous-alteration product, together with clay minerals (Brown et al. 2000; Zolensky et al. 2002), suggesting the occurrence of an aqueous process in its parent body (Kerridge et al. 1979). Mn–Cr age analyses of dolomites in the Tagish Lake meteorite have shown that the hydrothermal alteration in the Tagish Lake parent body occurred 4.5638–4.5625 billion years ago, which corresponds to 4.4–5.7 million years after the formation of the first minerals, calcium–aluminum-rich inclusions (CAIs; Connelly et al. 2012), in the solar nebula (Fujiya et al. 2013).

Remanent magnetization of minerals is very sensitive to the environments they experienced, including temperatures and

magnetic fields, during their formation and later, and is irreversible (Weiss et al. 2000). The recording of magnetic remanence is a process that adheres to Maxwell–Boltzmann statistics, and as such, the magnetic field recording grain population is significant in order to experimentally analyze this in a statistically significant sense. Magnetization relaxes from domains with smaller size and coercive force following

$$\tau = \frac{1}{C} \exp\left(\frac{VJ_s h_c}{2kT}\right), \quad (1)$$

where τ is the relaxation time of a magnetization, C is a constant value ($\sim 10^9$ s $^{-1}$ for magnetite), V is the volume of a magnetic domain, J_s is spontaneous magnetization, h_c is a microscopic coercive force, k is the Boltzmann constant, and T is the absolute temperature. The vortex magnetic domain structures especially are significantly stable for 10^{10} – 10^{11} yr or longer at room temperature, because the surface magnetic poles are hardly induced when a magnetic particle is divided into magnetic domains with spontaneous magnetization in the direction along the surface (Almeida et al. 2014; Shah et al. 2018).

On the other hand, lattice defects and internal stresses make an energy barrier that prevents the movement of the magnetic domain wall. The relaxation time of a magnetization depends on the activation energy, E , of these crystalline imperfections as

$$\tau = \frac{1}{C} \exp\left(\frac{E}{2kT}\right). \quad (2)$$

When a sample is heated to overcome the energy barrier, the magnetic moment moves accompanied by improving crystalline

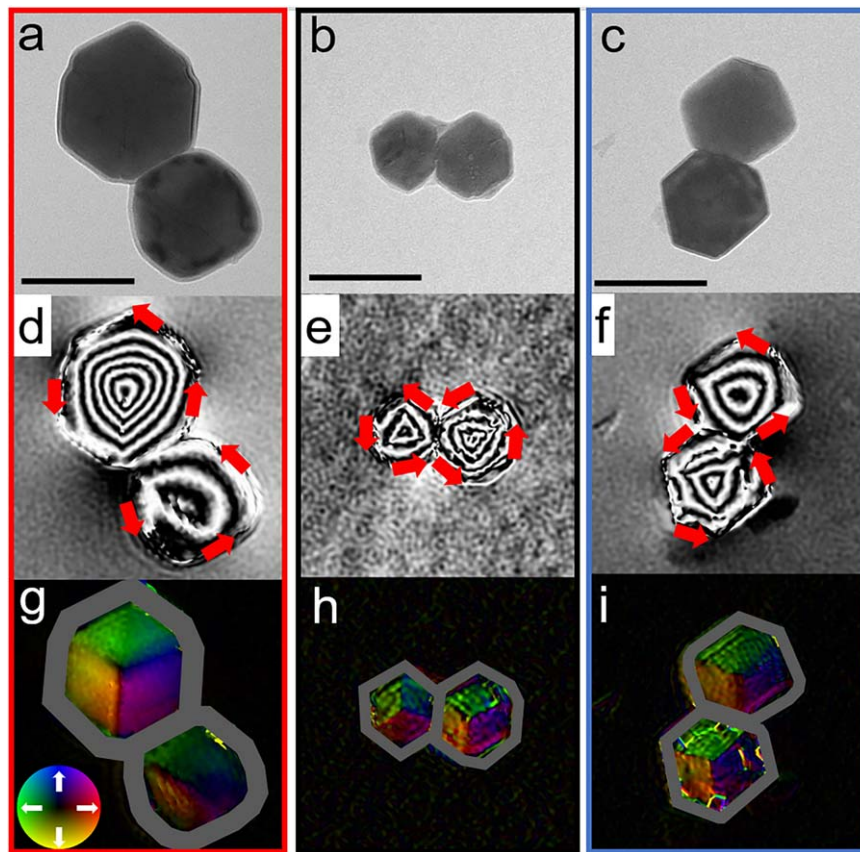


Figure 1. TEM images of magnetite particles from framboids. (a)–(c) Bright-field images taken before the annealing experiment. A rim on each particle is a carbon layer deposited to suppress electrical charging and physical movement. The scale bar is 200 nm. (d)–(f) Magnetic flux distribution images (two times (four times for (e)) the phase-amplified reconstruction) of (a)–(c) showing that each particle has a concentric circular magnetic field and a closed (i.e., vortex) structure. The red arrows indicate the directions of the magnetization vectors in the magnetite particles. (g)–(i) Color-wheel maps of the magnetization direction obtained from the reconstructed phase image, showing the domain structures. The white arrows in (g) show the direction of the magnetization in the color-wheel maps. The brightness of the colors indicates the strength of the magnetization vectors.

perfection. Consequently, here, we surmised that by applying the magnetic method through electron holography (Tonomura 1999) on a nanometer scale to minerals in a meteorite, it might be possible to elucidate the formation and/or thermal history of individual minerals. Here we describe our attempts to apply electron holography to magnetite nanoparticles extracted from the Tagish Lake meteorite. The nanometer-scale magnetism provided information pertaining to the history of the formation of its parent body and provided clues as to the early planetary dynamics of the outer solar system.

2. Results

2.1. Magnetic Properties of Magnetite

We selected clusters of framboids extracted from the Tagish Lake meteorite (see the Appendix) that had a typical rhombic-dodecahedral morphology (Nozawa et al. 2011) with sizes of approximately 100–250 nm in diameter (Figures 1(a)–(c)). The magnetization of the magnetite nanoparticles was examined by electron holography, which revealed that all the magnetite nanoparticles that we observed had a flux-closure vortex structure (Figures 1(d)–(i)). The samples were then annealed at 100°C in the microscope, and electron-interference patterns (holograms) were recorded after stabilization of thermal drift. The samples were subsequently cooled to room temperature and holograms were recorded once more.

This cycle of in situ observations was performed eight times at various temperatures up to 500°C in 50 or 100°C steps (Figures 2(b) and A1).

The brightness of the color-wheel map, which corresponds to the strength of the magnetic vector, was weaker at higher temperatures (e.g., 11 and 17 in Figure 2) than at room temperature (e.g., 12 and 18 in Figure 2). In contrast, the brightness increased after cooling to room temperature compared with that at the initial temperature (see Figures A2–A4 for all images). Magnetic flux densities, which were averaged for three domains in each particle, became 10%–20% higher for all magnetites upon thermal annealing (Figure 2(c)). The magnetic flux densities of the magnetites increased above the measurement deviation upon annealing at 300, 250, or 200°C (Figures 1(a), (b), and (c), respectively).

The decrease in the magnetic flux density at high temperatures is due to an intrinsic magnetic order/disorder phase transition as the Curie temperature (585°C for magnetite) is approached. After cooling to room temperature, the signal intensity can change for various reasons—for instance, a slight rotation of the particles, rotation of the vortex state, or alteration of saturation magnetization (see Suppl. Info. in Kimura et al. 2013). Indeed, the particles were sometimes observed to have moved in our initial experiments and, consequently, this was prevented by the deposition of an amorphous carbon layer before the heating experiment. If a particle rotates due to twisting or distortion of the TEM grid,

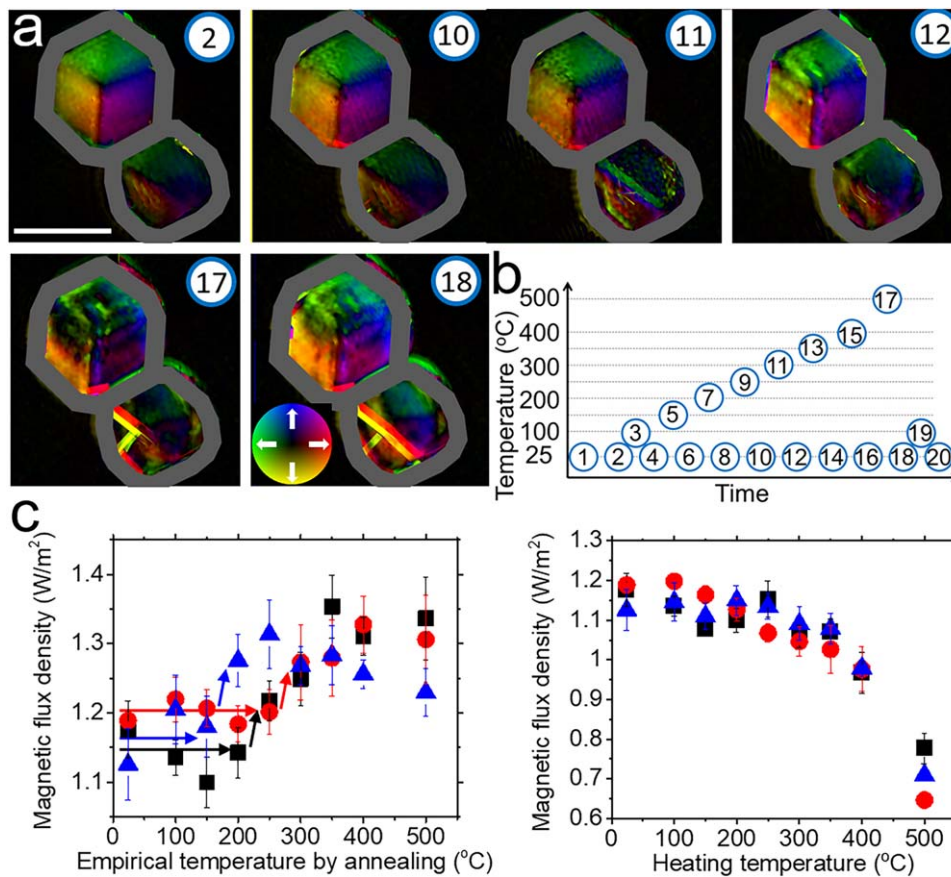


Figure 2. Strength of the magnetic vector dependence on the annealing temperature. (a) Color-wheel maps indicate the directions of the magnetic vectors obtained from the reconstructed phase images of the magnetite particles. The magnetization direction is shown by the white arrows in the color wheel. The brightness indicates the strength of the magnetic vector. The numbers in the blue circles show the recording sequence of the corresponding hologram. The scale bar is 200 nm. (b) Recording sequence of each image recorded at a temperature following the number in the blue circle. All corresponding color-wheel maps are presented in the Figures A2–A4. (c) Magnetic flux densities at room temperature after heating (left) and during heating (right). The values were averaged for domains in the particles. The red circle, black square, and blue triangle symbols correspond to the results for magnetite in Figures 1(a), (b), and (c), respectively. The error bars are derived from the measurement deviations for the six domains. The arrows are to guide the eye.

magnetic images such as those shown in Figure 2 cannot be obtained because the inner potential leading to a large phase signal on the electron wave cannot be subtracted precisely (see the Appendix). Although the rotation of the vortex state of a synthetic magnetite, preheated at 700°C, has been reported, the intensity decreases rather than increases above 400°C (Almeida et al. 2016). In our case, because all 24 magnetite particles showed an increase in magnetic intensity, an accidental increase as a result of the rotation of the vortex state is not plausible. The intensity in the saturation magnetization as a result of a change of oxidation state was not observed below 300°C in the vacuum conditions of the TEM (Almeida et al. 2016) and should be observed in all magnetites at the same temperature. One possible cause for the increase in the magnetic flux density of all magnetites at various temperatures is an increase in the saturation magnetization due to the alignment of the magnetic spin moment (Bryson et al. 2020). Perfect alignment was prevented by lattice defects, impurities, tiny magnetic domains, and/or internal stresses formed by imperfections in the crystal structure of the magnetite particle. Because the activation energies to relax those crystalline imperfections (Equation (2)) are different, the intensity could increase when the magnetite is heated above a temperature previously experienced.

The magnetic flux density of the magnetite in Figure 1(c) became higher at 200°C (blue triangles in Figure 2(c)). In contrast, that in Figure 1(a) showed no obvious change at 200°C (red circles in Figure 2(c)). The differences in the annealing temperatures that resulted in an increase in the magnetic flux density suggest that the magnetites had previously experienced different temperatures. The magnetites of Figures 1(a), (b), and (c) had not experienced temperatures above 300, 250, and 200°C, respectively. Exposure to a temperature of up to 250°C corresponds to the upper limit for the alteration temperature of the organic compounds in the Tagish Lake meteorite (Yabuta et al. 2010). Because all of these magnetites were extracted from the same piece of the meteorite, the temperature differences did not originate from an event that occurred after the formation of the magnetites. In other words, their remanent magnetization was acquired when they were formed. The magnetites in Figure 1(a) must have experienced temperatures of up to 250°C, whereas the magnetites in Figure 1(c) have never experienced a temperature as high as 200°C. Accordingly, during the cooling of the parent body of the Tagish Lake meteorite, the magnetites shown in Figure 1(a) were formed first at ~250°C and those shown in Figure 1(c) were formed subsequently at ~150°C.

2.2. Internal Heating Model for the Parent Body

To explore the heating processes for the formation temperature of the magnetites from 150°C to 250°C, we first modeled the internal heating of the parent body of the Tagish Lake meteorite, focusing on its accretion time and duration of heating. Because the Tagish Lake meteorite is a brecciated carbonaceous chondrite (Zolensky et al. 2002; Nakamura et al. 2003), the history of its parent body is complicated: It reaccreted from multiple fragments, possibly from impact ejecta. Because it is difficult to distinguish the magnetites formed before its reaccretion process from those formed later, we simply assumed a model for the intact nonporous parent body to obtain its formation time. We numerically solved a heat-conduction equation of the parent body that had a uniform composition of ice–rock mixture and a radius of 90 km, necessary to maintain a sufficiently high pressure for water to exist in the liquid phase at 250°C (see the Appendix). Note that the values for the initial water/rock ratio and the abundance of Al are based on published data for the Tagish Lake meteorite (Brown et al. 2000, 2002). When the water content is lower than what we used here, it can change the thermal properties and the amount of heat produced by the aqueous alteration. The temperature profile at a certain time may change from our current setting. Because earlier accreted bodies contain large amounts of one of the main heat sources (^{26}Al), they reach higher temperatures than those accreted later (Figure 3(a)). We also considered that the heat of the exothermic reaction due to aqueous alteration at 20°C provided an additional heat source to increase the peak temperature of the parent body (see the dashed line at 3.2 Myr in Figure 3(a)).

The blue-colored region in Figure 3(a) corresponds to the estimated peak temperature for the formation of framboidal magnetite. The green-colored region denotes the accretion time of the parent body of the Tagish Lake meteorite to form carbonate, such that the aqueous alteration occurred 4.4–5.7 Myr after the formation of the CAIs (Fujiya et al. 2013). In the case of the youngest body that satisfies the aqueous-alteration ages (i.e., accretion 3.1 Myr after the formation of CAIs), there is a temperature jump at 5.3 Myr, which is triggered by aqueous alteration (Figure 3(b); see Figure A5 for earlier accretion). Our estimated formation age around 3.0 Myr is consistent with the previous suggestion of 3.0–4.2 Myr (Sugiura & Fujiya 2014) regardless of our simple thermal modeling (see the Appendix). Note that additional chemical reactions would generate different reaction heat by producing other secondary minerals; this could alter the temperature evolution and the accretion time. Because the solubility of carbonate is inversely related to the temperature, supersaturation by carbonates increases with increasing temperature at the beginning of aqueous alteration, and precipitation subsequently occurs. In contrast, the solubility of magnetite is positively related to the temperature, and supersaturation of magnetite increases with decreasing temperature in the cooling stage of thermal metamorphic reactions.

2.3. Conditions for the Formation of Framboidal Magnetite

The formation temperatures of these magnetites differ by ~ 100 K. After aqueous alteration ceased, the temperature in the parent body started to decrease (Figures 3(b) and A5) because there was no additional heat source. It takes about two million years for the temperature to drop by 50 K at a distance

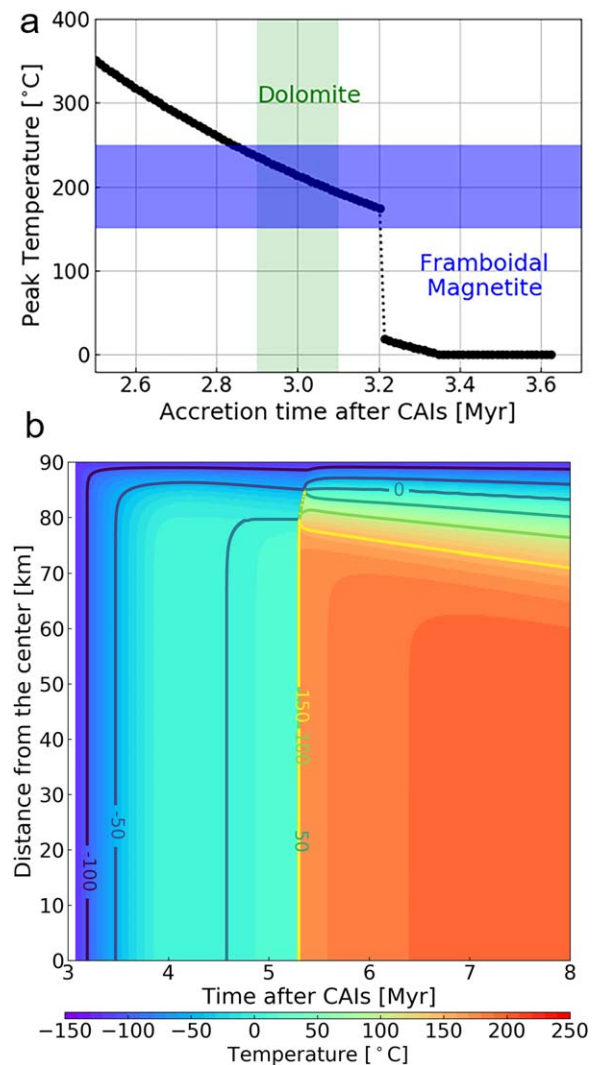


Figure 3. Temperature profile of a Tagish Lake–type body with a radius of 90 km. (a) The peak temperature depends on the accretion time after the formation of CAIs. The blue-colored region corresponds to the estimated peak temperature for the formation of framboidal magnetite. The green-colored region denotes the accretion time of the parent asteroid of the Tagish Lake meteorite such that the aqueous alteration occurred 4.4–5.7 Myr after the formation of CAIs (Fujiya et al. 2013). (b) Temperature evolution of a Tagish Lake–type body for the case in which the accretion time occurred 3.1 Myr after the formation of CAIs. The contour represents the temperature at each location in the parent body. Each line is drawn every 50°C. The temperature jumps throughout the body at 5.3 Myr were triggered by aqueous alteration.

of 75–80 km from the center of the body. Assuming there was no disruptive event, conductive cooling continues at the same rate. Therefore, a decrease in the interior temperature of the Tagish Lake parent body from 250 °C to 150 °C would have taken more than four million years. Note that the cooling proceeds much more slowly at locations nearer to the center of the body (i.e., duration of heating takes much longer). In order for magnetite in a framboid to have a broad size distribution, like the framboid of other carbonaceous chondrites, magnetite must grow at different degrees of supersaturation. Then, the formation of magnetite during prolonged cooling is understandable. In contrast, some framboids in the Tagish Lake meteorite are composed of magnetite particles with uniform size and morphology, which provides evidence that they were separately formed in a single event in isolated solutions in view

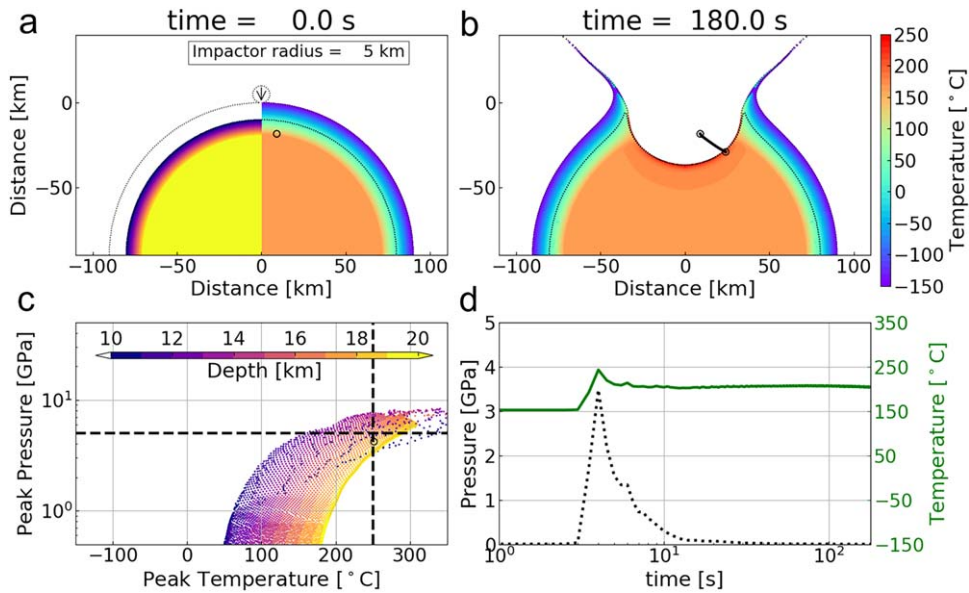


Figure 4. Temperature profiles for the shock heating of a thermally evolved Tagish Lake–type body with a radius of 90 km. This body is composed of a hydrous core with a radius of 80 km and a 10 km thick anhydrous crust. The anhydrous impactor has a radius of 5 km and a velocity of 5 km s^{-1} . (a) Initial temperature profile (right quarter circle) and depth color profile (left quarter circle) of the target body just after aqueous alteration (5.3 Myr after the formation of CAIs; see Figure 3(b)). Dotted lines show interfaces. A solid open circle shows one of the possible places that could be a suitable environment for the origin of the Tagish Lake meteorite. (b) Temperature profile 180 s after impact. The dumbbell shows the trajectory of the open circle in (a). (c) Peak temperature and pressure of the target body at various depths 180 s after impact. The horizontal and vertical dashed lines correspond to 5 GPa and 250°C , respectively. (d) Temperature (green solid line) and pressure (black dotted line) vs. time after impact at the position shown by the solid open circle in (a).

of the nucleation model (Nozawa et al. 2011; Kimura et al. 2013). Consequently, the formation condition of the framboid in the Tagish Lake meteorite is unique from that of the others. The larger size of the magnetites in Figure 1(a) is consistent with a higher formation temperature, where fewer crystalline nuclei are formed due to a lower supersaturation of the mother solution in the parent body at $\sim 250^\circ\text{C}$. The degree of supersaturation of the mother solution of the magnetites in Figure 1(c) increased as the temperature decreased; the magnetites finally nucleated at $\sim 150^\circ\text{C}$ after about four million years. It seems likely that a trigger such as a shock event induced simultaneous nucleation of the magnetites.

2.4. External Heating Model for the Formation of Magnetite at Various Temperatures

As the duration of internal heating is too long to form framboidal magnetite, we next studied the external heating for a rapid cooling scenario: An energetic impact might have provided a trigger for the nucleation event through shock. Indeed, signatures of various degrees of post-accretional alterations coexist in the Tagish Lake meteorite (Yabuta et al. 2010) and have been explained in terms of impact (Nakamura et al. 2003; Alexander et al. 2014). However, multiple collision events are not likely to have occurred, due to the very low collision frequency of only 10^{-7} every one million years for a 100 km object, as estimated from the conditions in the Trojans and in the asteroid belt (Levison et al. 2009). We therefore examined the effect of impacts on the parent body of the Tagish Lake meteorite in shortening the duration of thermal metamorphism by a shock event (Quirico et al. 2014), rather than examining the effects of shock in triggering nucleation at various temperatures of the parent body.

To reach a high temperature as a result of impact heating, the peak pressure must also increase (Kurosawa & Genda 2018;

Wakita & Genda 2019). The shock stage of the Tagish Lake meteorite is in the lowest category, S1, meaning that the Tagish Lake meteorite may have experienced a shock effect of less than 5 GPa (Brown et al. 2000). At such low pressures, it is hard to reach temperatures sufficiently high to trigger aqueous alteration (Figure A6). Because other chondrites such as CI, CR, and CM show signatures of aqueous alteration at a similar age, we assume that the aqueous alteration on the Tagish Lake parent body was also triggered by radiogenic internal heating rather than external impact heating. We therefore believe that impact on the aqueously altered body can explain the high temperature at a low shock stage for the Tagish Lake meteorite. We simulated impact heating in the parent body of the Tagish Lake meteorite just after aqueous alteration (see the Appendix). On the basis of our internal heating results (5.3 million years after the formation of CAIs in Figure 3(b)), we assume the existence of a parent body of radius 90 km with a secondary mineral core of radius 80 km and an anhydrous mineral crust (Figure 4(a)). Note that the energetic impact could also be the process that resulted in the formation of the Tagish Lake meteorite breccia.

If we knew the original location of the Tagish Lake parent body, we would be able to estimate its impact velocity. As it has been suggested that the location was in a region in or near the Kuiper Belt (Fujiya et al. 2019), we infer an impact velocity appropriate to that of an object near the orbit of Pluto. However, the velocity of typical impacts around the orbit of Pluto in the outer solar system is less than about 2 km s^{-1} (Zahnle et al. 2003). This would not have been enough to increase the internal temperature to 250°C . When the target body is porous, such low-velocity impacts can heat the matrix enough in the outer crust of the body during compaction (Bland et al. 2014). If this caused the formation of framboidal magnetite, it is expected that other secondary minerals have also formed at the same time. The secondary pyrrhotite along with magnetite in

the Tagish Lake meteorites (Zolensky et al. 2002) suggests this possibility; the impact-induced heating and aqueous alteration have happened contemporaneously. On the other hand, the similar formation time of secondary minerals (e.g., dolomite; Fujiya et al. 2013) in carbonaceous chondrites suggests that internal heating is more likely for aqueous alteration rather than impact-induced one. Thus, the low-velocity scenarios are less suitable for the Tagish Lake meteorite. Although the low shock stage is reported for the Tagish Lake meteorite (Brown et al. 2000; Zolensky et al. 2002), a larger impactor (10 km in radius) would have increased the peak pressure, except for limited conditions, as shown in Figure A7. However, when a rocky impactor of 5 km in radius collides at 5 km s^{-1} , a portion of the altered core can reach a temperature in excess of $250 \text{ }^\circ\text{C}$ (Figures 4(b)–(d)) while the peak pressure remains well below 5 GPa (Figures 4(c) and (d)).

In the case of a later collision, the temperature could have reached 250°C under conditions of lower pressure induced by a larger impactor. For instance, impact with a 10 km radius body is required for an impact event 7 million years after the formation of CAIs (Figure A8). However, this temperature increase would have occurred in a deeper place that would not have cooled down as efficiently. Therefore, an impact with a small impactor (5 km in radius) at 5 km s^{-1} is appropriate to provide conditions suitable for the formation of framboidal magnetite.

The additional impact heating on an aqueously altered body is a preferred scenario for a rapid cooling at a low pressure. As we have confirmed that the location satisfies the conditions of both temperature and pressure (a solid open circle in Figure 4(a) and in the bottom right area in Figure 4(c)), the temperature of a possible location of part of the Tagish Lake meteorite remained almost constant over 180 s after the impact (Figure 4(d)). There are two ways that the temperature could have decreased to as low as $\sim 150^\circ\text{C}$ in a relatively short period.

1. Assuming the layer above the candidate location for the Tagish Lake meteorite escaped from the body, the location would have been exposed to outer space. If we assume that the location depth was 10 m, the cooling time would be a few years, based on the typical thermal diffusivity of rock ($10^{-6} \text{ m}^2 \text{ s}^{-1}$).
2. If the Tagish Lake meteorite is assumed to have been excavated by the impact (Nakamura et al. 2003) and if the size of the ejected fragment was of the order of meters, the candidate for the Tagish Lake meteorite would have cooled within a few hundred hours.

Rapid cooling would also explain the relatively low abundances of amino acids in the Tagish Lake meteorite (Barge et al. 2019) despite the fact that its parent body possibly contained an aqueous solution that could have allowed the efficient formation of amino acids (White et al. 2020). The impact scenario therefore seems more plausible than the simple radiogenic internal heating model.

3. Discussion

These calculations suggest that, just after aqueous alteration, the parent body of the Tagish Lake meteorite experienced impact heating by a ~ 10 km diameter impactor at a velocity of $\sim 5 \text{ km s}^{-1}$, which is relatively common in the current main asteroid belt (Farinella & Davis 1992; Bottke et al. 1994). The

question remains as to whether this impact on the parent body of the Tagish Lake meteorite occurred in the cold outer solar system or after it had traveled to the outer main asteroid belt (or to the Trojan region; Levison et al. 2009; DeMeo & Carry 2014). Because the number density and impact velocity of solar system bodies would be larger in the latter case, the impact on the parent body of the Tagish Lake meteorite is more likely to have occurred in the main asteroid belt. The Tagish Lake parent body could therefore have migrated from the cold outer solar system to the outer main asteroid belt (Fujiya et al. 2019). If the Tagish Lake parent body formed through an instability process in the solar nebula, its size would be comparable with that of other bodies formed in a similar location (e.g., Johansen et al. 2014). The size of the Tagish Lake parent body required to maintain liquid water at 250°C is >160 km in diameter (see the Appendix), which is consistent with that of Kuiper Belt objects (Vilenius et al. 2014) rather than with that of comets (typically less than several tens of kilometers; Meech et al. 2004). Our results therefore indicate that the Tagish Lake parent object, which was originally located in the Kuiper Belt, might have experienced impact heating just after it had traveled to the main asteroid belt, which is a more plausible location for collisions to have occurred than the outer solar system. Note, however, that a rare collision event with a high impact velocity in the outer solar system might be possible. Because such impact events excavate hydrous minerals and/or ice, we might observe such an event as the birth of an active asteroid (Jewitt et al. 2015).

Our results represent that an impact on the Tagish Lake parent body occurred within 7 Myr (reasonably at 4.3–5.3 Myr) after the formation of CAIs. This time places constraints on the heliocentric dynamics in the solar system, possibly related to Jupiter, because Kuiper Belt objects might have been transported into the main asteroid belt during the dynamic migration of the giant planets (Walsh et al. 2011; Raymond & Izidoro 2017; Ribeiro et al. 2020), which occurred 0.5–2.5 Myr after their birth (Kruijer et al. 2017). If the Tagish Lake parent body traveled as a result of planetary migration, the giant planets were formed 1.8–4.8 Myr after the formation of CAIs. An early date for the formation of Jupiter is suggested by the isotopic dichotomy between carbonaceous and noncarbonaceous chondrites (Kruijer et al. 2017, 2020; Nanne et al. 2019). This dichotomy is a result of the formation of Jupiter’s core, which prevented mixing between materials of the inner and outer solar system ~ 1 –4 Myr after the formation of CAIs (Kruijer et al. 2020). During this period, the Tagish Lake parent body formed in the outer solar system at ~ 3 Myr and acquired its isotopic signature. The formation of Jupiter continued until ~ 4 –5 Myr (Kruijer et al. 2020), and it then induced inward migration of bodies from the outer solar system, including the Tagish Lake parent body. In this scenario, therefore, the suggested time for the formation of Jupiter is consistent with our impact age of within 7 Myr after the formation of CAIs. Scenarios for dynamic migrations in the solar system have been debated, and a wide range of periods between a few Myr and 650 Myr have been suggested (Voosen 2020); however, the calculated impact age of the Tagish Lake parent body is consistent with the scenario discussed above and supports an early formation of Jupiter.

We gratefully acknowledge the developers of iSALE-2D, including Gareth Collins, Kai Wünnemann, Dirk Elbeshausen,

Tom Davison, Boris Ivanov, and Jay Melosh, and the developer of the pySALEPlot tool, Tom Davison. Numerical computations were carried out on the PC cluster and analysis servers at the Center for Computational Astrophysics of the National Astronomical Observatory of Japan. This work was supported by Grants-in-Aid for Challenging Exploratory Research and Scientific Research (S) from KAKENHI (16K13909 and 20H05657).

Appendix

Data and materials availability. All data are available in the main text or in the supplementary materials. At present, iSALE-2D is not fully open source; it is distributed on a case-by-case basis to academic users in the impact community, strictly for noncommercial use. Scientists interested in using or developing iSALE code may apply at the iSALE web page (<http://www.isale-code.de>). Our input files are available on the website (<https://doi.org/10.5281/zenodo.5102964>). The thermal modeling output will be available from S.W. upon reasonable request.

Sample Treatments. The pristine fragments of the Tagish Lake meteorite that we obtained were collected without magnets a few days after the fall of the meteorite and were purchased from La Memoire de la Terre SARL, France. A piece ($\sim 1 \text{ mm}^3$) of the Tagish Lake meteorite with a carbonate-poor lithology that contained magnetite more abundantly than other carbonate-rich lithologies (Zolensky et al. 2002) was gently grained together with ethanol in an agate mortar. The grained powder was poured into a 10 ml glass bottle filled with ethanol using a polypropylene pipette, and the mixture was agitated by ultrasound. A 5–10 μl aliquot of the suspension was taken with a polypropylene pipette and dropped onto a thin film of amorphous carbon supported on a standard copper grid of a transmission electron microscope (TEM). Thus, all tools we used to prepare the samples are nonmagnetic. To prevent electron charging and physical rotation of the sample during a series of experiments, an amorphous carbon layer about 5 nm thick was deposited, which has been seen as a rim on each grain surface (Figures 1(a)–(c)).

Analytical method using TEM. TEM images and holograms were recorded by an electron-holography TEM (Hitachi High-Tech, HF3300-EH) with an acceleration voltage of 300 kV, located at the Japan Fine Ceramics Center. All TEM observations are performed in an additional sample stage maintained in a magnetic-field-free environment (less than 17 μT , which is in the direction opposite to the electron beam). The TEM grid, with magnetite extracted from the Tagish Lake meteorite, was loaded into the magnetic-field-free sample stage by using a heated-stage specimen holder of the TEM (Figure A1). Several types of magnetite, including framboids, plaquettes, and euhedral single grains, were observed. Because of their suitable size, their transparency to electrons, and the ease with which magnetite could be distinguished from many other mineral particles, we selected clusters of framboidal magnetites. Observed particles, except for the bottom particle shown in Figure 1(a), were oriented in the [1–10] direction in the TEM. Three or four holograms were taken with a $4\text{K} \times 4\text{K}$ CCD camera ($0.244 \text{ nm pixel}^{-1}$ on the sample plane) and these were integrated for precise reconstruction of each observation. The exposure time was 40 s for each hologram. The reconstructed object wave of electrons that passed through the TEM sample contained information not only on the magnetic flux, but also on the inner potential of the sample.

Because the thickness of the magnetite particles was not uniform, these two components could not be separated in a single image. To extract the magnetic flux component for a sample, we also observed the reconstructed object wave from the opposite side after inverting the sample, because this inverted the direction of the Lorentz force. The sign of the phase change arising from the magnetic component became opposite to the original, whereas the phase change arising from the inner potential component remained the same. By subtracting the reconstructed phase, we eliminated the electric inner potential of the sample.

We examined 24 magnetite particles in three heating runs. We could not correctly subtract the inner potential from the hologram images of 18 magnetite particles in the first two runs due to the rotation or movement of the particles caused by thermal effects, because we intended to use holograms recorded at above the Curie temperature (585°C) to subtract the inner potential. Nevertheless, it was confirmed that the magnetic flux densities of all magnetite particles increased after heating at 300°C in the first two runs.

The bottom particle in Figure 1(a) does not show three symmetrical domains clearly because of the tilting of the crystallographic orientation relative to the electron beam. Consequently, we show the results for five magnetite particles (Figures 1(a)–(c)). Even for these five magnetite particles, measurement of their magnetic flux densities was not easy at higher temperature because of incomplete subtraction of the inner potential due to subtle rotation or movement of the particles or substrate at high temperatures. In particular, the measurement error for magnetic flux densities increased at higher temperature above 400°C . The development of a stabilization technique will be important in establishing a nanometer-scale magnetic method using electron holography.

Note that the amplification of the subtracted phase image produces a magnetic component that is double that obtained from a single image. We recorded the first hologram (Circle 1 in Figure 2(b)) from one side of the sample and the second hologram (Circle 2 in Figure 2(b)) from the other side after inverting the sample. The internal potential was removed by subtraction of the phase changes reconstructed from these two holograms to retrieve the magnetic information. The contour-line map of the reconstructed phase image corresponds to the magnetic flux distribution (Figures 1(d)–(f)). To generate the color-wheel map showing the magnetic domain structures, x and y differential values of the phase image were calculated, and the vector directions are displayed as different colors (Figures 1(g)–(i) and A2–A4). See Kimura et al. (2013) for more-detailed explanations.

Thermal Modeling of the Parent Body of the Tagish Lake Meteorite. To determine the temperature conditions for the formation of the magnetites, we modeled the thermal evolution of the parent body of the Tagish Lake meteorite. This model has been used to produce thermal models of comets, Kuiper Belt objects, and parent bodies of chondrites (Gounelle et al. 2008; McKinnon et al. 2008; Gail et al. 2014; Lichtenberg et al. 2016; Monteux et al. 2018). Here, we adopted the same method as that developed in previous work (Wakita & Sekiya 2011) because the model can handle aqueous alteration as a source of additional heat to that generated by the decay of ^{26}Al . We assumed the parent body to be a spherical rocky body with an initial temperature of -123°C (150 K). By assuming an initial water (ice)-to-rock mass ratio of 0.21 (inferred from a porosity of $\sim 37\%$; Brown et al. 2002), we considered the latent heat of

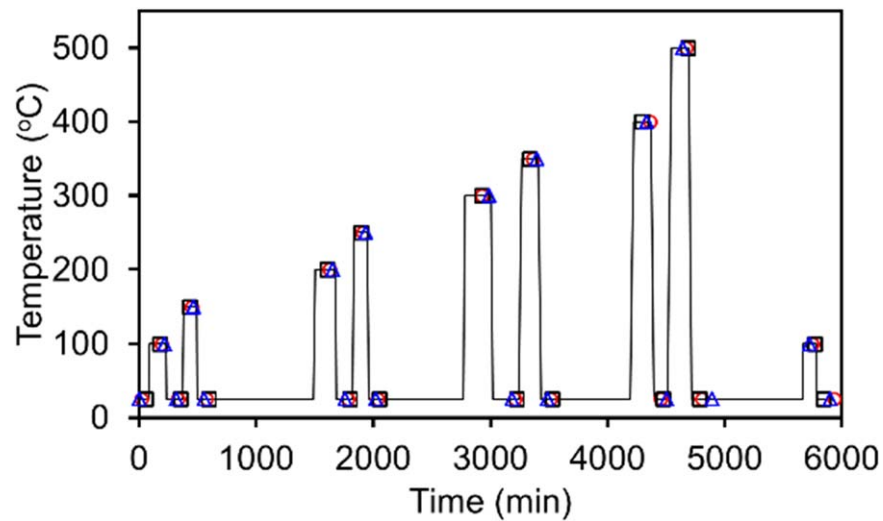


Figure A1. Temperature profile for the heating experiment shown in Figures 2 and A2–A4. The black line shows the temperature profile. The red circle, black square, and blue triangle show the times for the recordings of the electron holograms (interference fringe patterns) shown in Figures A2–A4, respectively. The ambient temperature during the observation was 22.9–24.7°C. Electron holograms (interference fringe patterns) are usually recorded under low electron-dose conditions to improve the coherence of incident electron waves. The electron-dose rate in our measurement was of the order of 10^2 electrons $\text{nm}^2 \text{s}^{-1}$, which is 10^2 – 10^6 times lower than that in conventional high-resolution TEM observations. Therefore, the temperature variation due to electron irradiation was negligible compared with the accuracy of $\pm 10^\circ\text{C}$ of a double-tilting heating specimen holder for TEM. The heating and cooling rates were in the range of 11– $20^\circ\text{C} \text{ minute}^{-1}$. The waiting time required to stabilize the movement of the sample at each annealing temperature was between 50 and 210 minutes. The samples were not irradiated by electrons during the waiting times.

ice melting and the heat of the exothermic reactions due to aqueous alteration. For the sake of simplicity, we assumed the following constant values for the physical properties of rock, ice, and water; thermal conductivities of 1, 2.2, and $0.56 \text{ J m}^{-1} \text{ s}^{-1} \text{ K}^{-1}$; specific heats of 910, 1900, and $4200 \text{ J kg}^{-1} \text{ K}^{-1}$; and densities of 2700, 1000, and 1000 kg m^{-3} , respectively (Yomogida & Matsui 1983; Murphy & Koop 2005; National Astronomical Observatory of Japan 2010; Opeil et al. 2010). The heat-conduction equation was solved numerically by a finite-difference method and by an explicit method of time integration. Although the parent body of Tagish Lake meteorites can be originally located in Kuiper Belt, we assumed the body as a generous carbonaceous chondritic parent body. Thus, our modeling has some deficit regarding Kuiper Belt objects, such as a temperature-dependent thermal conductivity for ice and low density (Bierson & Nimmo 2019; Castillo-Rogez et al. 2019). Nevertheless, as we noted in the main text, the formation time of the parent body of Tagish Lake meteorites by our model is similar to predicted formation time based on the $\varepsilon^{54}\text{Cr}$ of the meteorites (Figure 3; Sugiura & Fujiya 2014). Therefore, our thermal modeling as the Tagish Lake parent body is sufficient.

When the lithostatic pressure is above the pressure of water vapor, liquid water can exist. The lithostatic pressure at the center of a parent body depends on its radius and has values of 0.5, 2.1, and 4.8 MPa for bodies of radius 30, 60, and 90 km, respectively. Note that our setup of a water/rock ratio of 0.21 results in a bulk density of 2070 kg m^{-3} . At locations in the body further away from the center, the pressure decreases. The vapor pressure of water depends on the temperature and at 250°C is about 3.5–4.0 MPa (Sonntag 1994; National Astronomical Observatory of Japan 2010). A body of radius 77–82 km would have pressures of this magnitude at its center. Similar lithostatic pressures and vapor pressures at 250°C would be found 47–35 km from the center of a body of radius 90 km. We therefore adopted 90 km as a reasonable radius for

the parent body to ensure a sufficiently high pressure for the preservation of water in the liquid phase (Figure A5).

Some parameters such as the initial temperature and the water/rock ratio have the potential to change the thermal history of the body (e.g., Cohen & Coker 2000; Castillo-Rogez & McCord 2010; Neumann et al. 2020). However, changing those parameters would be comparable to shifting the formation time, e.g., a 100 K change of the initial temperature corresponds to a 0.1 Myr shift in the formation time (Wakita et al. 2014). We therefore fixed these parameters and only varied the accretion time of the parent body, which determines the initial ratio of $^{26}\text{Al}/^{27}\text{Al}$. Although some thermal modeling has considered the growth of the parent body (Merk et al. 2002; Ghosh et al. 2003; Castillo-Rogez & McCord 2010; Vernazza et al. 2014; Wakita et al. 2014; Neumann et al. 2020), the formation process of planetesimals is still in debate (Johansen et al. 2007, 2014, 2015). We therefore simply considered the final parent body without any further growth (i.e., instant formation due to an instability process; Johansen et al. 2007, 2014). Note that the initial temperature and/or the hydrothermal circulation (Bland & Travis 2017) could affect the temperature profile. Thus, the thickness of the outer anhydrous crust would be varied (see below).

Impact Heating in the Parent Body of the Tagish Lake Meteorite. We simulated an impact on the parent body of the Tagish Lake meteorite, which had experienced aqueous alteration in its core (Figures 4 and A6–A10), by using the iSALE-2D shock-physics code (Amsden et al. 1980; Collins et al. 2004; Wünnemann et al. 2006) iSALE-Dellen version (Collins et al. 2016). Based on our thermal modeling of a 90 km body, the radius of the hydrous core was assumed to be 80 km with an anhydrous mineral crust 10 km thick. We set the initial temperature profile of the target body to a similar profile to that indicated by the results of our thermal modeling. Note that the timescale of an impact on the parent body is much shorter than the typical timescale of radiogenic heating (several million years).

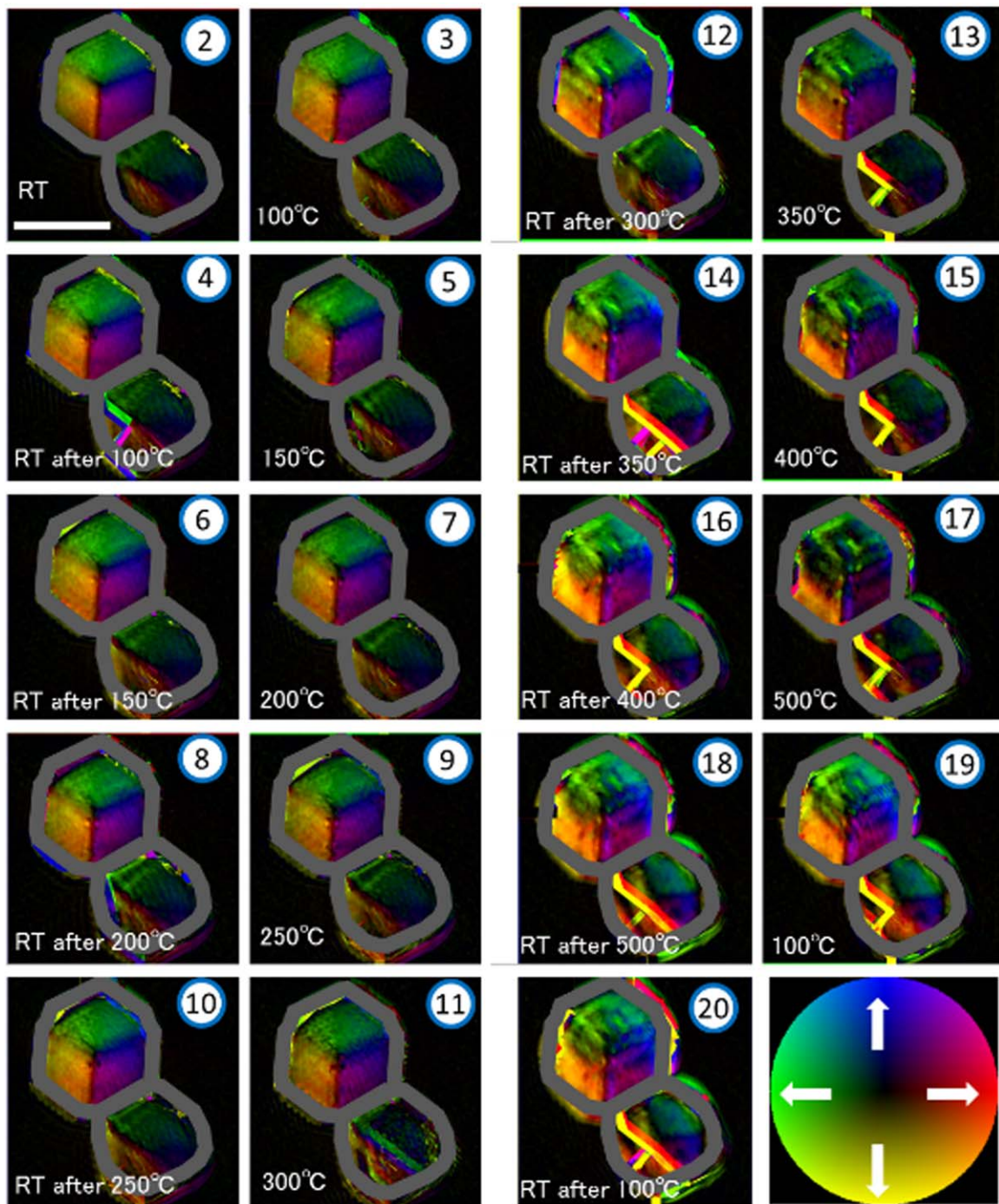


Figure A2. Dependence of the strength of magnetic vectors on the annealing temperature. Color-wheel map of the magnetization direction obtained from the reconstructed phase images of magnetite particles extracted from a framboid. The numbers in blue circles show the recording sequence of the corresponding holograms. Each image was recorded at the temperature shown in Figure 2(b). The color and brightness in the profiles of the magnetites indicate the direction and strength of the magnetic vectors, respectively. The corresponding TEM image are indicated in Figure 1(a). The white arrows show the direction of the magnetization direction of the color wheel. The scale bar is 200 nm.

We therefore ignored the effects of radiogenic heating in our impact simulations.

To describe the state of a material over a wide thermodynamic domain, impact simulations require the material's equation of state. For this purpose, the analytic equation of state (ANEOS) is included in iSALE, but the range of available materials is very limited. Because the Tagish Lake meteorite contains carbonates as aqueously altered materials, we chose calcite (Pierazzo et al. 1998) as a model secondary mineral for the hydrous core to

represent the physical properties of hydrous materials. Because the pressure/temperature profile of dunite is similar to that of minerals in ordinary chondrites (Svetsov & Shuvalov 2015), dunite can serve as a model to represent an anhydrous mineral crust for these impact simulations (e.g., Johnson et al. 2015). We therefore adopted dunite (Benz et al. 1989) as the anhydrous mineral for both the impactor and anhydrous crust. We used the iSALE input parameters given by Collins et al. (2008). The choice of material in the ANEOS code changes the

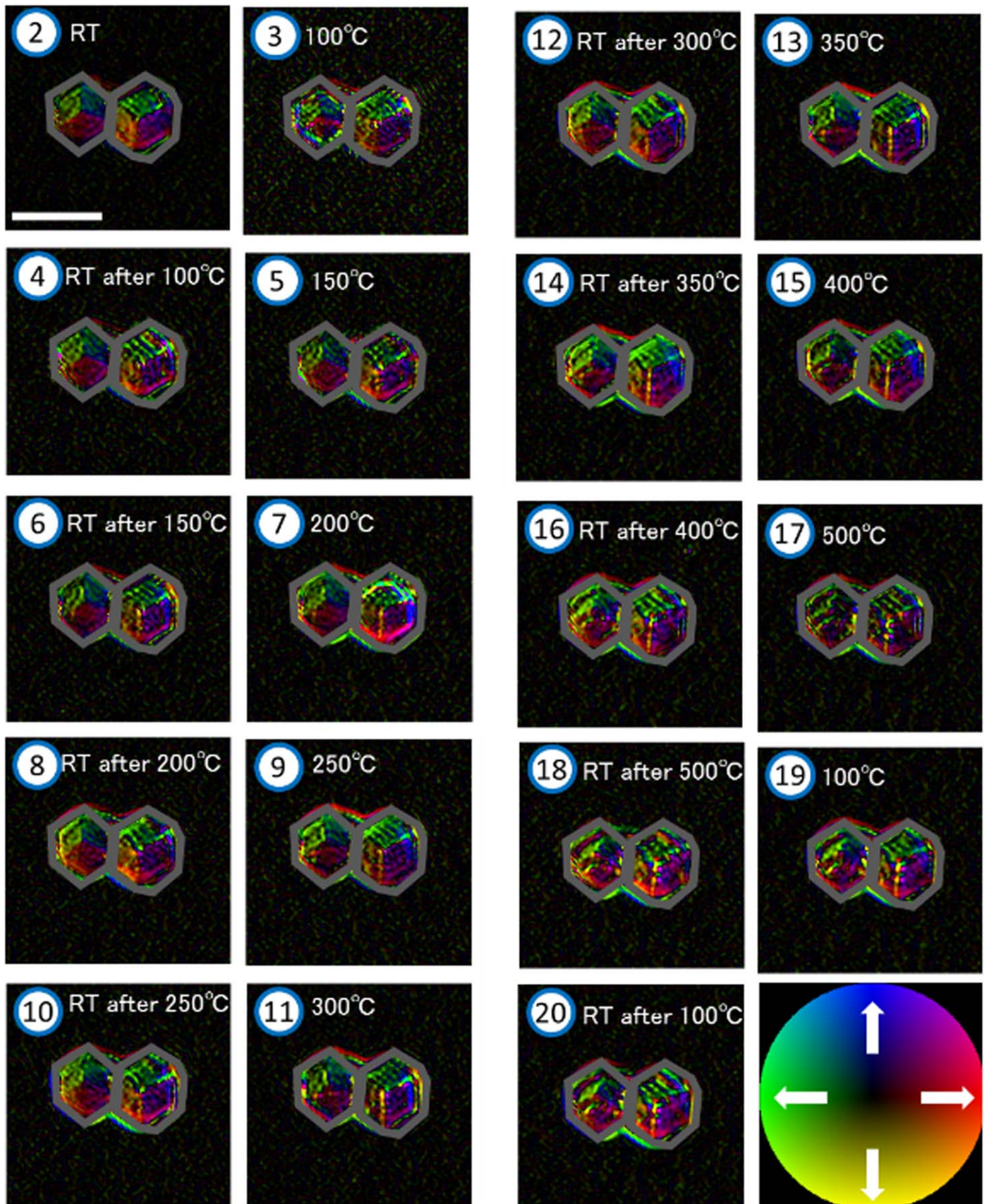


Figure A3. Dependence of the strength of magnetic vectors on the annealing temperature. As in Figure A2, except for the corresponding TEM image, which is Figure 1(b). The scale bar is 200 nm.

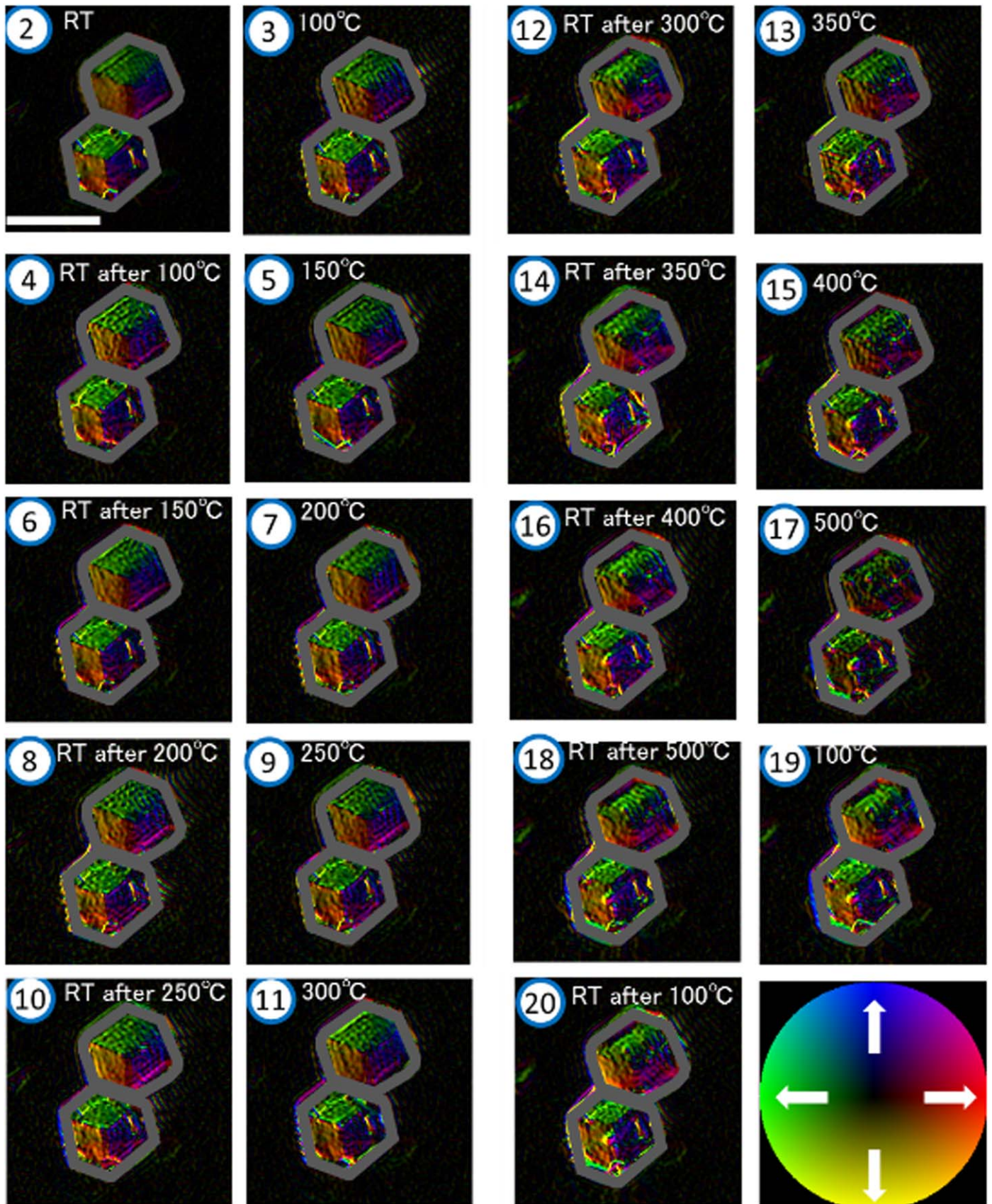


Figure A4. Dependence of the strength of the magnetic vector on the annealing temperature. As in Figure A2 except for the corresponding TEM image, which is Figure 1(c). The scale bar is 200 nm.

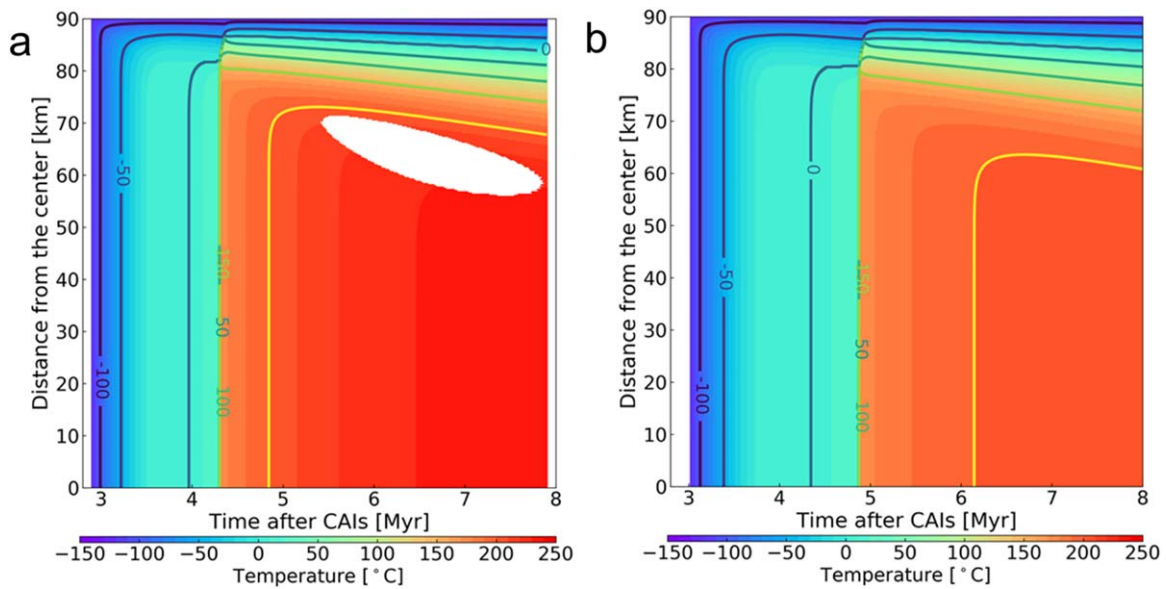


Figure A5. Temperature evolution of a Tagish Lake–type body with a radius of 90 km. The contours represent the temperature at each position of the parent body. The lines are drawn every 50°C; the yellow line corresponds to 200°C. (a) Accretion at 2.9 Myr after the formation of CAIs. (b) Accretion at 3.0 Myr after the formation of CAIs. The temperature jumps at 4.3 and 4.9 Myr are triggered by aqueous alteration. The white region in (a) shows the environment in which water will vaporize.

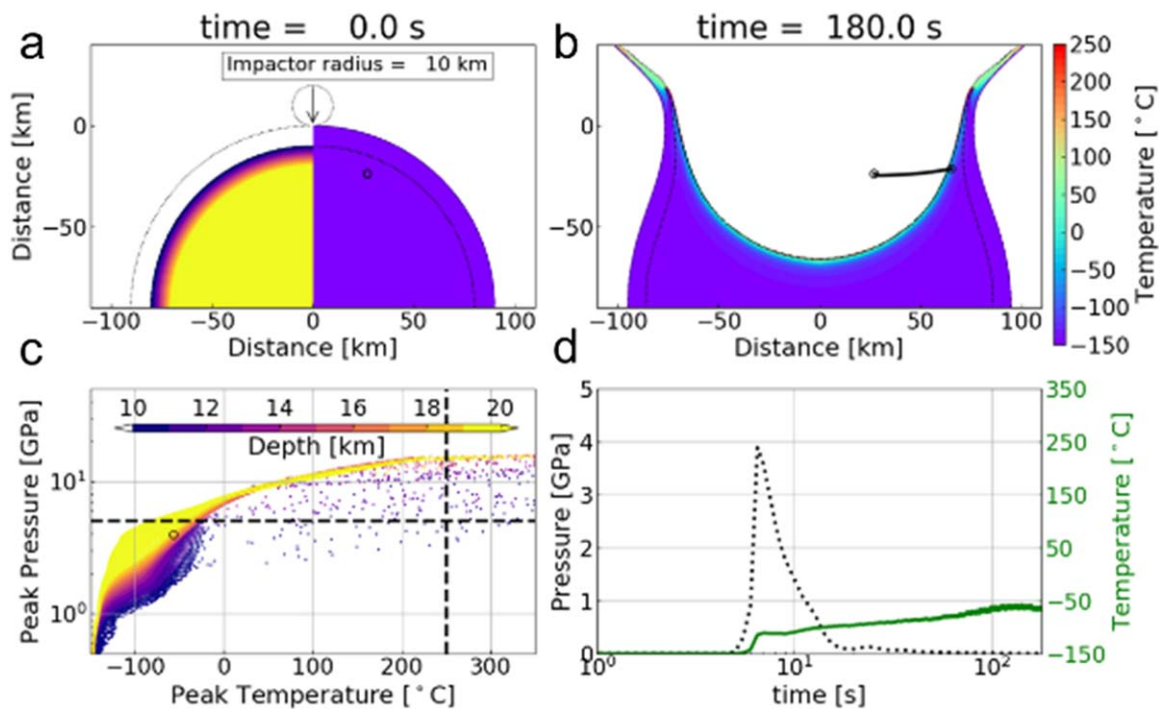


Figure A6. Temperature profiles for the shock heating of a Tagish Lake–type body with a radius of 90 km. As in Figure 4, except for the size of the anhydrous impactor (radius 10 km) and the initial temperature profile, which was assumed to be uniform at -123°C . Note that some points in the regions of pressure and temperature below 5 GPa and 250°C , respectively, in (c) are artifacts: there is no position in the body that satisfies conditions where the temperature reaches 250°C and the pressure remains below 5 GPa.

pressure/temperature relationship during impact. As a result, the specific location for the origin of the Tagish Lake meteorite might also change (Figures A9 and A10; Wakita & Genda 2019). The choice of thickness of the outer anhydrous crust is another influential parameter. Although we take it to be 10 km thick based on our thermal modeling results, it

might change depending on the conditions of thermal modeling (see above). The thicker crust would prevent temperature increases in a hydrous core (Wakita & Genda 2019). However, our conclusion that impact on an aqueously altered body could trigger the formation of magnetite is still valid.

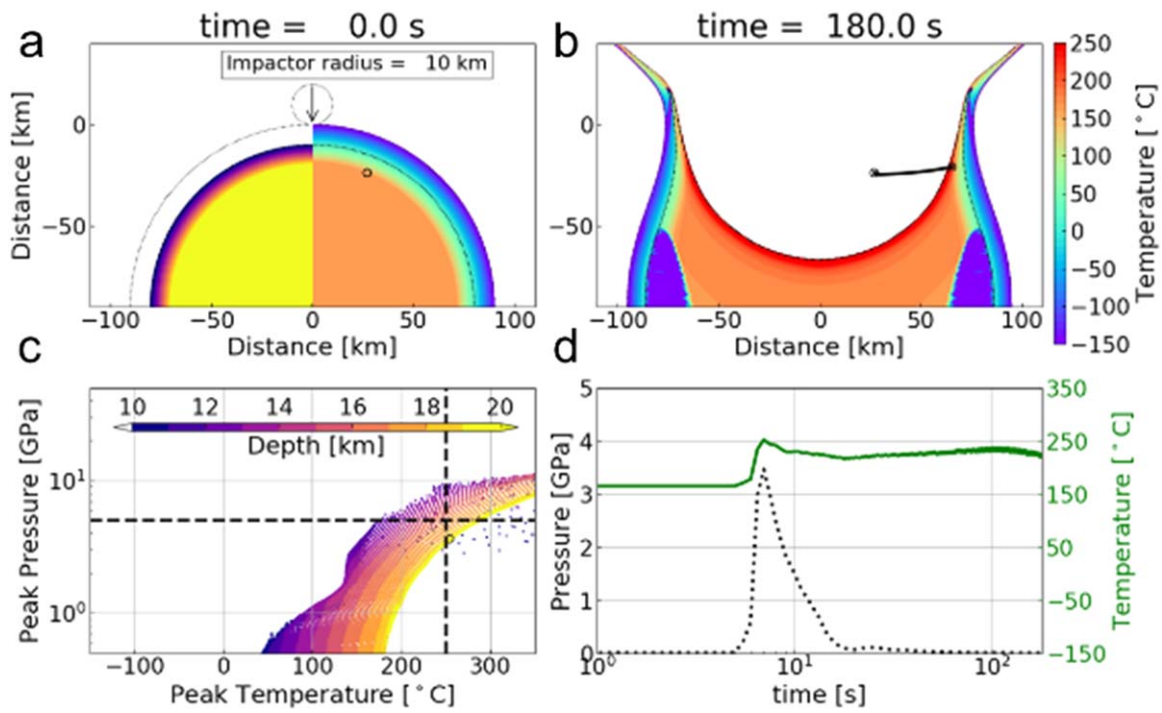


Figure A7. Temperature profiles for the shock heating of a thermally evolved Tagish Lake-type body with a radius of 90 km. As in Figure 4, except for the size of the anhydrous impactor, which has a radius of 10 km.

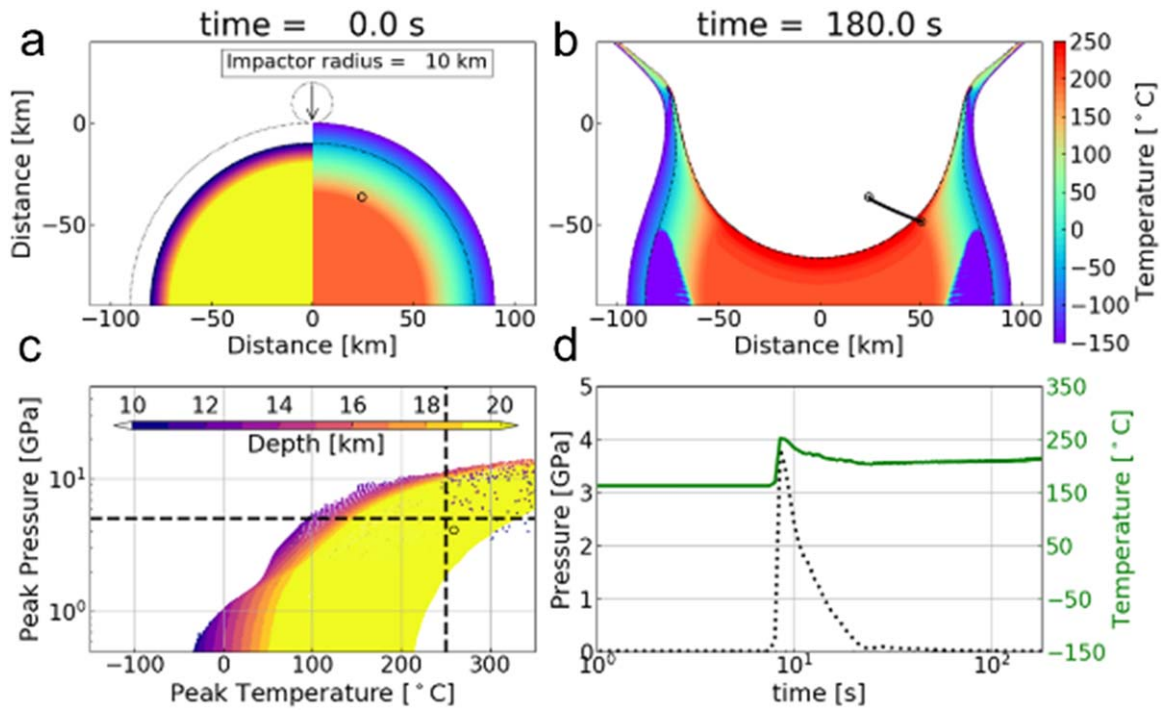


Figure A8. Temperature profiles for the shock heating of a thermally evolved Tagish Lake-type body with a radius of 90 km. As in Figure 4, except for the size of the anhydrous impactor, which has a radius of 10 km, and the initial temperature profile of the target body 7 Myr after the formation of CAIs; see Figure 3(b).

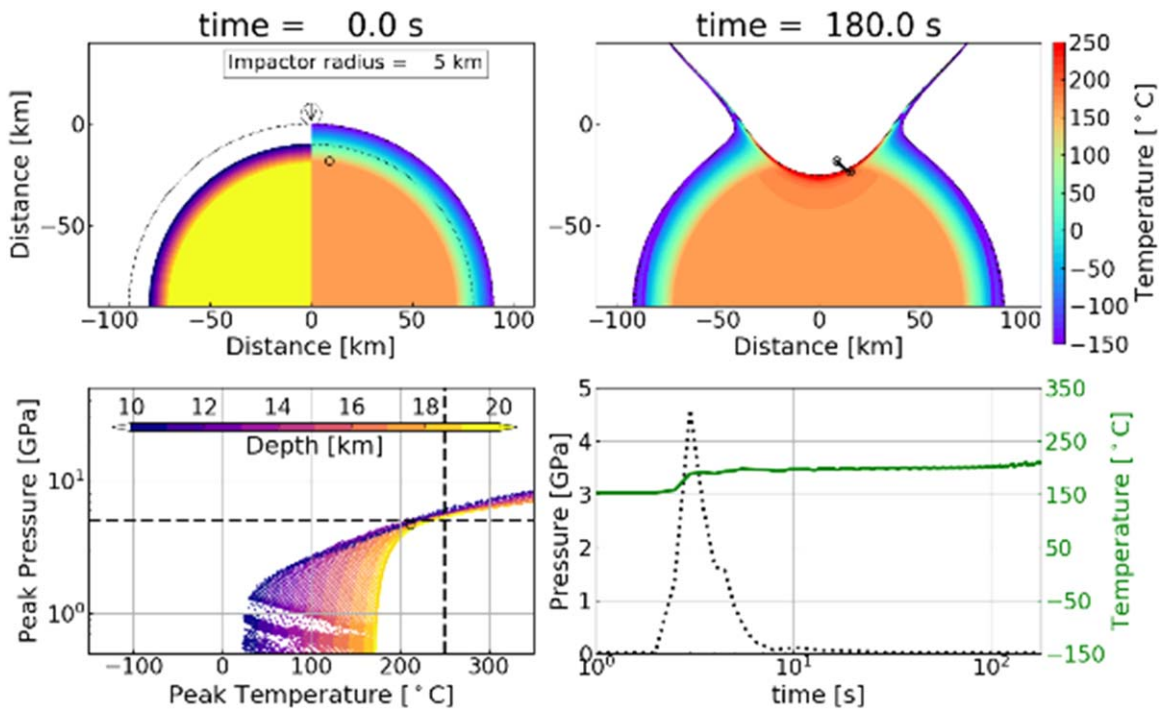


Figure A9. Temperature profiles for the shock heating of a thermally evolved Tagish Lake–type body with a radius of 90 km. As in Figure 4, except for the anhydrous core, to examine how composition affects the results.

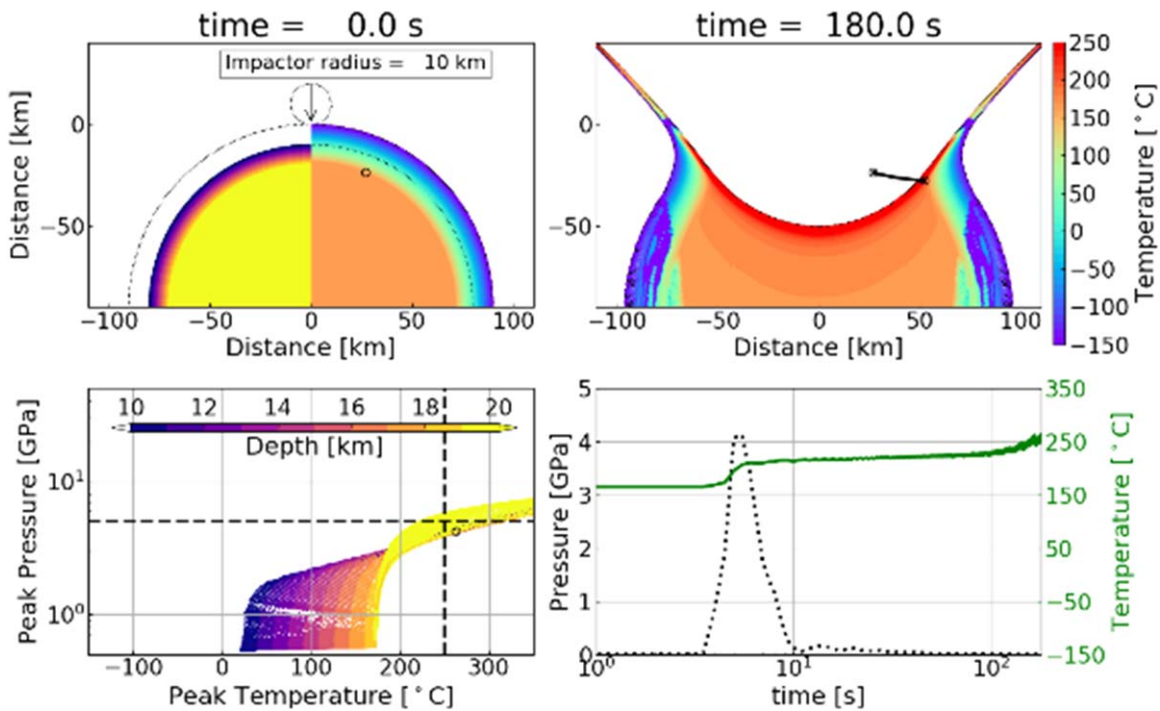


Figure A10. Temperature profiles for the shock heating of a thermally evolved Tagish Lake–type body with a radius of 90 km. As in Figure A7, except for the anhydrous core, to examine how composition affects the results.

ORCID iDs

Yuki Kimura  <https://orcid.org/0000-0002-9218-7663>
 Shigeru Wakita  <https://orcid.org/0000-0002-3161-3454>

References

- Alexander, C. M. O'D., Cody, G. D., Kebukawa, Y., et al. 2014, *M&PS*, **49**, 503
- Almeida, T. P., Kasama, T., Muxworthy, A. R., et al. 2014, *GeoRL*, **41**, 7041
- Almeida, T. P., Muxworthy, A. R., Kovács, A., et al. 2016, *GeoRL*, **43**, 8426
- Amsden, A., Ruppel, H., & Hirt, C. 1980, SALE: A Simplified ALE Computer Program for Fluid Flow at all Speeds. Los Alamos National Laboratories Report, LA-8095:101p, Available at https://inis.iaea.org/collection/NCLCollectionStore/_Public/11/571/11571883.pdf
- Barge, L. M., Flores, E., Baum, M. M., VanderVelde, D. G., & Russell, M. J. 2019, *PNAS*, **116**, 4828
- Benz, W., Cameron, A., & Melosh, H. 1989, *Icar*, **81**, 113
- Bierson, C. J., & Nimmo, F. 2019, *Icar*, **326**, 10
- Bland, P., Collins, G., Davison, T., et al. 2014, *NatCo*, **5**, 5451
- Bland, P. A., & Travis, B. J. 2017, *SciA*, **3**, e1602514
- Bottke, W. F., Nolan, M. C., Greenberg, R., & Kolvoord, R. A. 1994, *Icar*, **107**, 255
- Brown, P. G., Hildebrand, A. R., Zolensky, M. E., et al. 2000, *Sci*, **290**, 320
- Brown, P. G., ReVelle, D. O., Tagliaferri, E., & Hildebrand, A. R. 2002, *M&PS*, **37**, 661
- Bryson, J. F. J., Weiss, B. P., Lima, E. A., Gattacceca, J., & Cassata, W. S. 2020, *ApJ*, **892**, 126
- Castillo-Rogez, J., Vernazza, P., & Walsh, K. 2019, *MNRAS*, **486**, 538
- Castillo-Rogez, J. C., & McCord, T. B. 2010, *Icar*, **205**, 443
- Cohen, B. A., & Coker, R. F. 2000, *Icar*, **145**, 369
- Collins, G. S., Elbeshhausen, D., Wünnemann, K., et al. 2016, Manual for the Dellen release of the iSALE shock physics code10, Available at <https://doi.org/10.6084/m9.figshare.3473690.v2>
- Collins, G. S., Melosh, H. J., & Ivanov, B. A. 2004, *M&PS*, **39**, 217
- Collins, G. S., Morgan, J., Barton, P., et al. 2008, *E&PSL*, **270**, 221
- Connelly, J. N., Bizzarro, M., Krot, A. N., et al. 2012, *Sci*, **338**, 651
- DeMeo, F., & Carry, B. 2014, *Natur*, **505**, 629
- Farinella, P., & Davis, D. R. 1992, *Icar*, **97**, 111
- Fujiya, W., Hoppe, P., Ushikubo, T., et al. 2019, *NatAs*, **3**, 910
- Fujiya, W., Sugiura, N., Sano, Y., & Hiyagon, H. 2013, *E&PSL*, **362**, 130
- Gail, H. P., Trieloff, M., Breuer, D., & Spohn, T. 2014, in *Protostars and Planets IV*, ed. H. Beuther et al. (Tucson, AZ: Univ. Arizona Press), 571
- Ghosh, A., Weidenschilling, S. J., & McSween, H. Y., Jr. 2003, *M&PS*, **38**, 711
- Gounelle, M., Morbidelli, A., Bland, P. A., et al. 2008, in *The Solar System Beyond Neptune*, ed. M. A. Barucci et al. (Tucson, AZ: Univ. Arizona Press), 525
- Grimm, R. E., & McSween, H. Y., Jr. 1993, *Sci*, **259**, 653
- Jewitt, D., Hsieh, H., & Agarwal, J. 2015, in *Asteroids IV*, ed. P. Michel, F. E. DeMeo, & W. F. Bottke (Tucson, AZ: Univ. Arizona Press), 221
- Johansen, A., Blum, J., Tanaka, H., et al. 2014, in *Protostars and Planets VI*, ed. H. Beuther et al. (Tucson, AZ: Univ. Arizona Press), 547
- Johansen, A., Mac Low, M.-M., Lacerda, P., & Bizzarro, M. 2015, *SciA*, **3**, E1500109
- Johnson, B. C., Minton, D. A., Melosh, H. J., & Zuber, M. T. 2015, *Natur*, **517**, 339
- Johansen, A., Oishi, J. S., Mac Low, M.-M., et al. 2007, *Natur*, **448**, 1022
- Kerridge, J. F., Mackay, A. L., & Boynton, W. V. 1979, *Sci*, **205**, 395
- Kimura, Y., Sato, T., Nakamura, N., et al. 2013, *NatCo*, **4**, 2649
- Kruijjer, T. S., Burkhardt, C., Budde, G., & Kleine, T. 2017, *PNAS*, **114**, 6712
- Kruijjer, T. S., Kleine, T., & Borg, L. E. 2020, *NatAs*, **4**, 32
- Kurosawa, K., & Genda, H. 2018, *GeoRL*, **45**, 620
- Levison, H. F., Bottke, W. F., Gounelle, M., et al. 2009, *Natur*, **460**, 364
- Lichtenberg, T., Golabek, G. J., Gerya, T. V., & Meyer, M. R. 2016, *Icar*, **274**, 350
- McKinnon, W. B., Prialnik, D., Stern, S. A., & Coradini, A. 2008, in *The Solar System Beyond Neptune*, ed. M. A. Barucci et al. (Tucson, AZ: Univ. Arizona Press), 213
- Meech, K. J., Hainaut, O. R., & Marshen, B. G. 2004, *Icar*, **170**, 463
- Merk, R., Breuer, D., & Spohn, T. 2002, *Icar*, **159**, 183
- Monteux, J., Golabek, G. J., Rubie, D. C., Tobie, G., & Young, E. D. 2018, *SSRv*, **214**, 39
- Murphy, D. M., & Koop, T. 2005, *QJRM*, **131**, 1539
- Nakamura, T., Noguchi, T., Zolensky, M. E., & Tanaka, M. 2003, *E&PSL*, **207**, 83
- Nanne, J. A. M., Nimmo, F., Cuzzi, J. N., & Kleine, T. 2019, *E&PS*, **511**, 44
- National Astronomical Observatory of Japan 2010, *Chronological Scientific Tables (Maruzen)* (in Japanese) (Tokyo: Maruzen Co., Ltd.)
- Neumann, W., Jaumann, R., Castillo-Rogez, J., Raymond, C. A., & Russell, C. T. 2020, *A&A*, **633**, A117
- Nozawa, J., Tsukamoto, K., van Enckevort, W., et al. 2011, *JChS*, **133**, 8782
- Opeil, C. P., Consolmagno, G. J., & Britt, D. T. 2010, *Icar*, **208**, 449
- Pierazzo, E., Kring, D. A., & Melosh, H. J. 1998, *JGR*, **103**, 28607
- Quirico, E., Bonal, L., Beck, P., et al. 2018, *GeCoA*, **241**, 17
- Quirico, E., Orthous-Daunay, F.-R., Beck, P., et al. 2014, *GeCoA*, **136**, 80
- Raymond, S. N., & Izidoro, A. 2017, *Icar*, **297**, 134
- Ribeiro, R. de S., Morbidelli, A., Raymond, S. N., et al. 2020, *Icar*, **339**, 113605
- Rubin, A. F. 2012, *GeCoA*, **90**, 181
- Shah, J., Williams, W., Almeida, T. P., et al. 2018, *NatCo*, **9**, 1173
- Sonntag, D. 1994, *MetZe*, **3**, 51
- Sugiura, N., & Fujiya, W. 2014, *M&PS*, **49**, 772
- Svetsov, V. V., & Shuvalov, V. V. 2015, *P&SS*, **117**, 444
- Tomomura, A. 1999, *Electron Holography* (Berlin: Springer)
- Vernazza, P., Zanda, B., Binzel, R. P., et al. 2014, *ApJ*, **791**, 120
- Vilenius, E., Kiss, C., Müller, T., et al. 2014, *A&A*, **564**, A35
- Voosen, P. 2020, *Sci*, **367**, 350
- Wakita, S., & Genda, H. 2019, *Icar*, **328**, 58
- Wakita, S., Nakamura, T., Ikeda, T., & Yurimoto, H. 2014, *M&PS*, **49**, 228
- Wakita, S., & Sekiya, M. 2011, *EP&S*, **63**, 1193
- Walsh, K. J., Morbidelli, A., Raymond, S. N., O'Brien, D. P., & Mandell, A. M. 2011, *Natur*, **475**, 206
- Weiss, B. P., Kirschvink, J. L., Baudenbacher, F. J., et al. 2000, *Sci*, **290**, 791
- White, L. F., Tait, K. T., Langelier, B., et al. 2020, *PNAS*, **117**, 11217
- Wünnemann, K., Collins, G. S., & Melosh, H. J. 2006, *Icar*, **180**, 514
- Yabuta, H., Alexander, C. M. O., Fogel, M. L., Kilcoyne, A. L. D., & Cody, G. D. 2010, *M&PS*, **45**, 1446
- Yomogida, K., & Matsui, T. 1983, *JGR*, **88**, 9513
- Zahnle, K., Schenk, P., Levison, H., & Dones, L. 2003, *Icar*, **163**, 263
- Zolensky, M. E., Nakamura, K., Gounelle, M., et al. 2002, *M&PS*, **37**, 737